Journal of Magnetism and Magnetic Materials 485 (2019) 271–279

Contents lists available at ScienceDirect

Journal of Magnetism and Magnetic Materials

journal homepage: www.elsevier.com/locate/jmmm

Research articles

The structure, electrical and magnetic properties of M-doped $PbPdO_2$ (M = Cu, Co, Fe) thin films: A first-principles and experimental study

Jian-Min Zhang[a,b], Xiang Chen[a,c], Hai Jia[a,c], Yanmin Yang[a,c], Shuiyuan Chen[a,c], Zhigao Huang[a,b,*]

[a] Fujian Provincial Key Laboratory of Quantum Manipulation and New Energy Materials, College of Physics and Energy, Fujian Normal University, Fuzhou 350117, China
[b] Fujian Provincial Collaborative Innovation Center for Optoelectronic Semiconductors and Efficient Devices, Xiamen 361005, China
[c] Fujian Provincial Engineering Technical Research Centre of Solar Energy Conversion and Stored Energy, Fuzhou 350117, China

ARTICLE INFO

Keywords:
$PbPdO_2$
Transition metal doping
PLD
Magnetism
Resistivity
First-principles calculations

ABSTRACT

$PbPdO_2$ and M-doped $PbPdO_2$ (M = Cu, Co, Fe) films were prepared using pulsed laser deposition (PLD) method. The structures, electrical and magnetic properties were systematically investigated by XRD, Raman, SEM, XPS, AFM and VSM. Our results indicate that $PbPdO_2$ and $PbPd_{0.9}M_{0.1}O_2$ (M = Cu, Co, Fe) film with (0 0 2) preferred orientation can be well fabricated. The valence states of magnetic atoms in M-doped $PbPdO_2$ (M = Cu, Co, Fe) thin films are identified to be Cu^{1+}, $Co^{2+,3+}$ and Fe^{3+}, respectively. All $Pb(Pd,M)O_2$ (M = Cu, Co, Fe) films exhibit ferromagnetism with high metal-insulator transition temperatures at around 330–370 K. Moreover, the resistivity of Fe doped $PbPdO_2$ film is higher than that of the pristine $PbPdO_2$ film, while the resistivities of Co and Cu doped $PbPdO_2$ films are lower. At the same time, Fe, Co and Cu dopants do enhance the ferromagnetism of $PbPdO_2$ film, while the enhancement of magnetic moment for Fe dopant is most evident. Lastly, based on Pb vacancy and O^{-1} observed experimentally, the band gaps and magnetic moments of $Pb(Pd,M)O_2$ films were calculated by first-principles, and the results explain well the experimental facts.

1. Introduction

A novel class of materials named spin gapless semiconductor (SGS) was proposed by Wang in 2008 [1]. The exotic character that both electron and hole can be fully spin-polarized in these materials highlights the application potential in spintronic or electronic devices [2,3]. The SGS, which bridges semiconductors and half-metals, has generated great interest including $PbPdO_2$-based semiconductors [4-14] and Heusler alloys [15], such as CoFeMnSi (T_C = 620 K) [16] and Mn_2CoAl [17], CoFeCrGa [18] and Fe_2CoSi [19].

Particularly, Co-doped $PbPdO_2$ exhibits many extraordinary properties, such as high-temperature ferromagnetism [4], colossal electroresistance (CER) [5] and giant magnetoresistance (GMR) [5,20,21]. These fascinating properties make Co-doped $PbPdO_2$ to be a prospective spintronic material. Experimentally, magnetic properties of Co doped $PbPdO_2$ have been reported by Jung et al. [20,21]. Su et al. have prepared the $PbPd_{0.81}Co_{0.19}O_2$ film using sol-gel spin-coating technique, and the room temperature ferromagnetism was also observed [4,11,22]. $PbPdO_2$ was also found to be a *p*-type gapless semiconductor with intrinsic hole carriers, and the unusual high-temperature ferromagnetism was reported in Co-doped $PbPdO_2$ [6,23]. Co-doped $PbPdO_2$ films were also prepared by pulsed laser deposition (PLD) technique, and their magnetotransport and magnetoresistance were studied [9,10,24].

Different magnetic atoms have been introduced into $PbPdO_2$ for modulating the physics properties of SGSs. Single-phase samples of Cu doped $PbPdO_2$ have been synthesized via solid-state reaction, and a metal-insulator transition was identified [25,26]. Similar metal-insulator-like transitions were reported in Co and Mn doped $PbPdO_2$, with the transition temperature of 150 K and 70 K, respectively. In addition, Co doping enhanced the ferromagnetic interactions, whereas Mn doping favors antiferromagnetic in $PbPdO_2$ [21]. Kim et al. [8] found that Co-doped $PbPdO_2$ was indeed a small-gap semiconductor, while the phase separation was observed in the Mn doped $PbPdO_2$. $PbPd_{0.9}Zn_{0.1}O_2$ and $PbPd_{0.9}Cu_{0.1}O_2$ were revealed to exhibit diamagnetic and paramagnetic, respectively [10]. Fe [27], Mn [28] and Ni

* Corresponding author at: Fujian Provincial Key Laboratory of Quantum Manipulation and New Energy Materials, College of Physics and Energy, Fujian Normal University, Fuzhou 350117, China.
E-mail address: zghuang@fjnu.edu.cn (Z. Huang).

https://doi.org/10.1016/j.jmmm.2019.04.084
Received 15 October 2018; Received in revised form 4 April 2019; Accepted 24 April 2019
Available online 25 April 2019

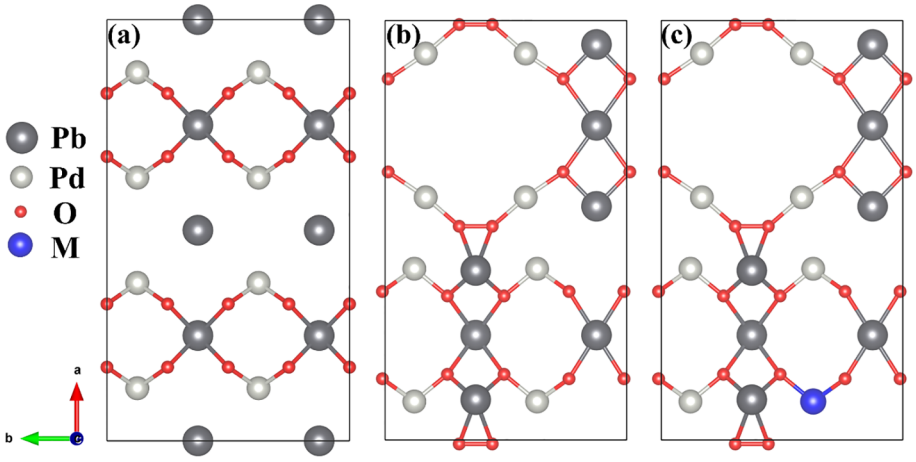

Fig. 1. The crystal structure of $PbPdO_2$: (a) pure, (b) with vacancies, (c) with vacancies and doping. A unit cell containing 32 atoms and the blue atoms M represents magnetically doped atoms (Cu, Co, Fe).

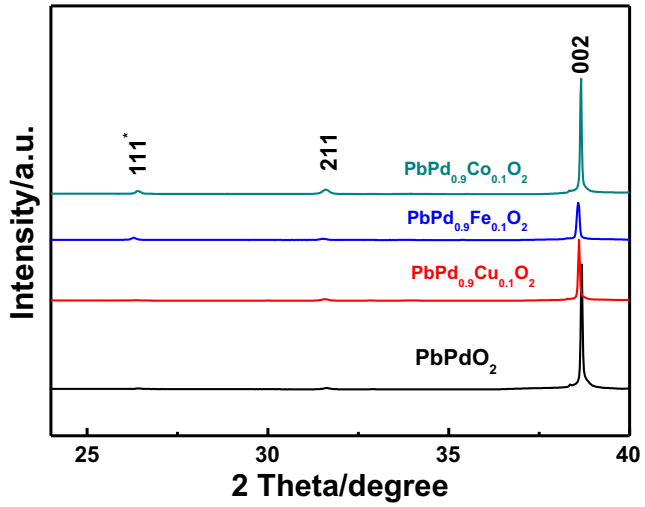

Fig. 2. XRD patterns of $PbPdO_2$ and $PbPd_{0.9}M_{0.1}O_2$ (M = Cu, Co, Fe) films.

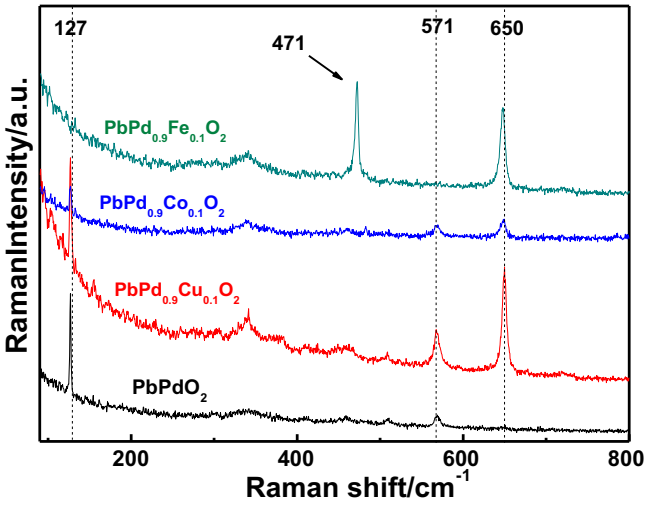

Fig. 3. Raman spectra of $PbPdO_2$ and $PbPd_{0.9}M_{0.1}O_2$ (M = Cu, Co, Fe) films.

[29] doped $PbPdO_2$ can be also synthesized by sol-gel spin-coating method. High-temperature ferromagnetism was reported in Fe and Ni doped $PbPdO_2$ nanograin films [10,27], while ferromagnetism and antiferromagnetism were found to coexist in Mn doped films [28].

However, although many studies have been found in transition metal doped $PbPdO_2$, up to now, high quality thin films of doped $PbPdO_2$ is still difficultly prepared. Especially, great difficulties still should be conquered upon the growth of preferred orientation. Furthermore, the origin of intriguing magnetism in transition metal doped $PbPdO_2$ is still elusive and controversial. Consequently, it is crucial to study systematically the structure, electrical and magnetic properties for different transition metal doped $PbPdO_2$.

In this paper, based on the prepared experimentally high quality thin films, combined with first-principles calculations, the structures, electrical and magnetic properties of the M-doped $PbPdO_2$ (M = Cu, Co, Fe) thin films have been studied. The PLD method was adopted to fabricate the $PbPdO_2$ and $PbPd_{0.9}M_{0.1}O_2$ (M = Cu, Co, Fe) films with (0 0 2) preferred orientation. The element concentration and valence states of M-doped $PbPdO_2$ (M = Cu, Co, Fe) thin films were characterized. Temperature-dependent resistivity curves show that Fe doped film has higher resistivity than the pristine $PbPdO_2$, while Co and Cu doped films have lower resistivity. All samples possess a wide temperature of metal-insulator transition (T_{MI}) at around 330–370 K. Finally, four samples exhibit the room ferromagnetism, while the magnetic moment of $PbPd_{0.9}Fe_{0.1}O_2$ is the largest. Our theoretical calculated results confirm the experimental observations.

2. Materials and methods

2.1. Synthesis of $PbPd_{0.9}M_{0.1}O_2$ (M = Cu, Co, Fe)

The $PbPd_{0.9}M_{0.1}O_2$ (M = Cu, Co, Fe) bulk samples synthesized by sol-gel method were used as the PLD target. $Pb(NO_3)_2$, $Pd(NO_3)_2$, $Cu(NO_3)_2$, $Co(NO_3)_2$ and $Fe(NO_3)_2$ were used as raw materials. The chelating agent and solvent were citric acid monohydrate and deionized water, respectively. An additional 5 mol % $Pb(NO_3)_2$ was used to supplement the volatilization of Pb in the process of the subsequent heating treatment. The thin films were deposited on the substrate of (1 0 0) oriented MgO single crystal by PLD technique. A KrF excimer laser with a wavelength of 248 nm was used as a source of target ablation and the

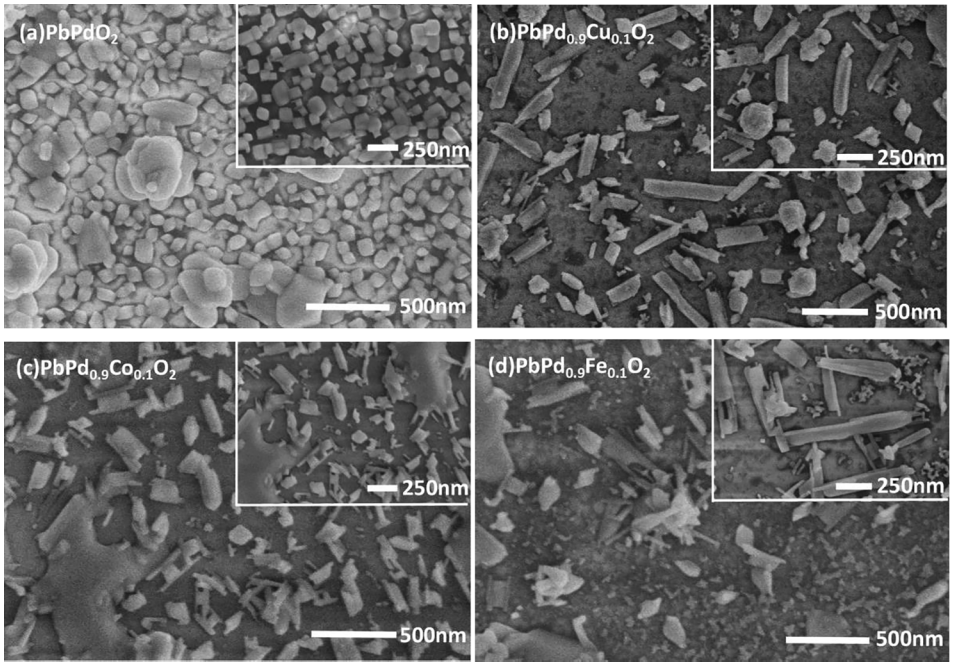

Fig. 4. SEM images of $PbPdO_2$ and $PbPd_{0.9}M_{0.1}O_2$ (M = Cu, Co, Fe) films.

Table 1
Element concentrations of $PbPdO_2$ and $PbPd_{0.9}M_{0.1}O_2$ (M = Cu, Co, Fe) film.

Sample	O K	Pb M	Pd L	Cu K	Co K	Fe K
$PbPdO_2$	60.60	13.37 (0.81)	15.98	0	0	0
$PbPd_{0.9}Cu_{0.1}O_2$	68.75	11.86 (0.71)	15.13	1.52 (Cu^{1+})	0	0
$PbPd_{0.9}Co_{0.1}O_2$	67.82	14.23 (0.79)	16.32	0	1.63 ($Co^{2+,3+}$)	0
$PbPd_{0.9}Fe_{0.1}O_2$	64.63	16.20 (0.85)	17.92	0	0	1.25 (Fe^{3+})

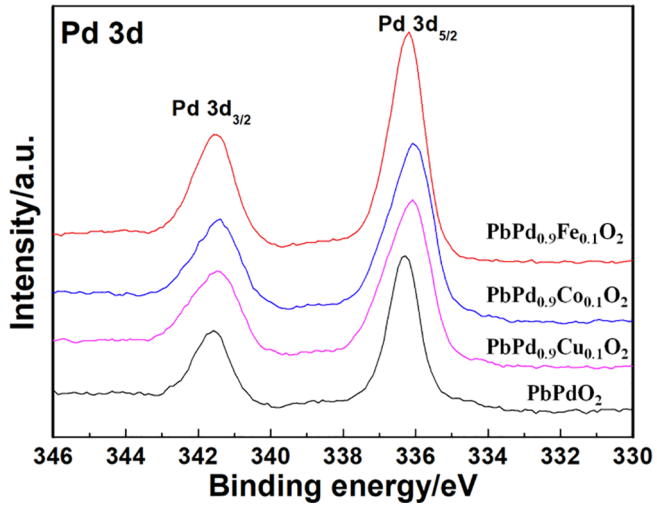

Fig. 5. XPS spectra of Pd 3d for $PbPdO_2$ and $PbPd_{0.9}M_{0.1}O_2$ (M = Cu, Co, Fe) films.

repetition rate is 3 Hz. The deposited time was 30 min, and the thickness of the samples is about 400 nm. The substrate temperature is 550 °C. After deposition, the samples were ex-situ annealed with 6 h in air at 650 °C.

2.2. Characterization methods

The powder X-ray diffraction patterns (XRD) of $PbPdO_2$ were characterized by Rigaku Ultima (Cu Kα, λ = 0.15418 nm). The Scanning Electron Microscopy (SEM) was characterized by Hitachi SU-8010. The Raman spectroscopy was recorded at room temperature using HORIBA Jobin Yvon Evolution with laser excitation at 532 nm. The electronic properties were measured by semiconductor characterization systems (HALL8686). The surface morphologies and work functions of $PbPdO_2$ and $PbPd_{0.9}M_{0.1}O_2$ (M = Cu, Co, Fe) thin films were characterized using atomic force microscopy (AFM, Bruker Dimension). X-ray photoelectron spectra (XPS) were measured by Thermo Fisher ESCALAB250Xi, and the binding energy of the XPS spectra was calibrated. The magnetic properties were measured by VersLab.

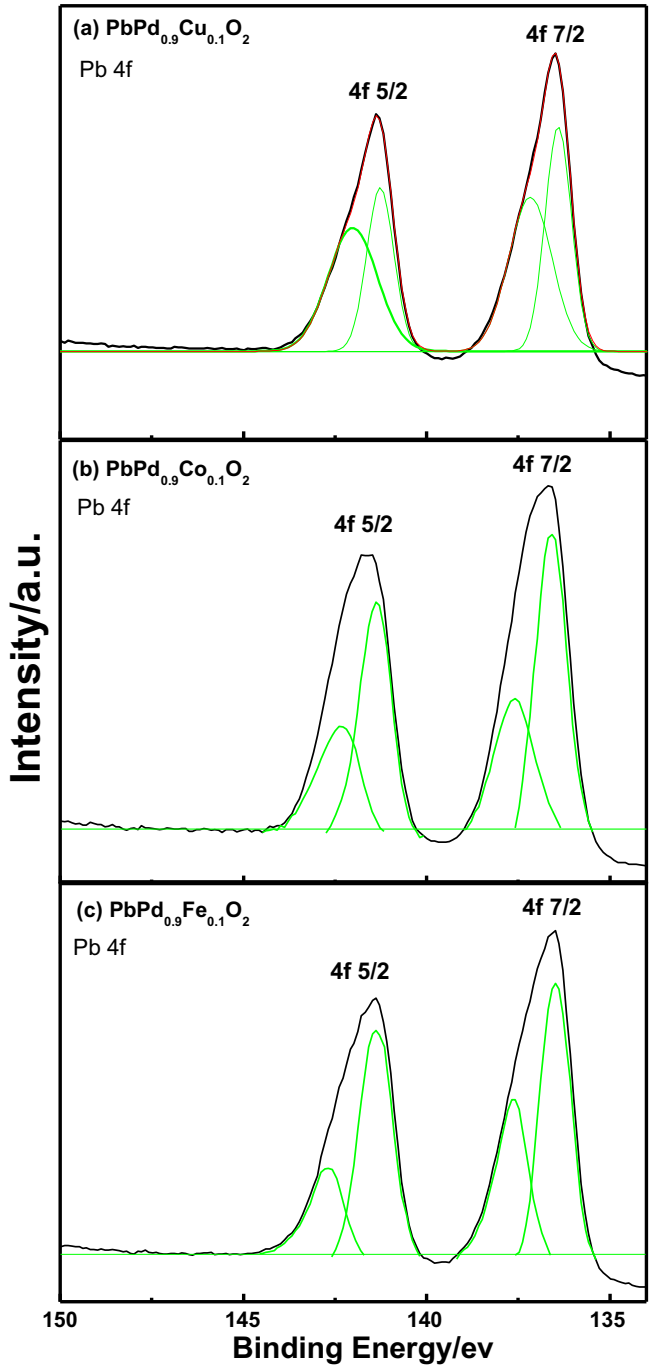

Fig. 6. XPS spectra of Pb 4f for $PbPdO_2$ and $PbPd_{0.9}M_{0.1}O_2$ (M = Cu, Co, Fe) films.

2.3. First-principles method

Our first-principles calculations were carried out by using Vienna *ab initio* simulation package (VASP) [30,31], and the pseudopotential plane-wave method with projected augmented wave potentials was used [32]. Perdew-Burke-Ernzerhof (PBE) formulation of generalized gradient approximation (GGA) for exchange-correlation functional was implemented [33,34]. The cutoff energy was set to 550 eV. A 6 × 8 × 1 Monkhorst k-point mesh was adopted for 2 × 2 × 1 $PbPdO_2$ (0 0 2) film supercells. To simulate the two-dimensional infinite sheet, periodic boundary condition was used. The slab with 15 Å vacuum layer was adopted for $PbPdO_2$ (0 0 2) film with the experimental lattice constants of a = 9.572 Å, b = 5.508 Å and c = 4.751 Å. Fig. 1 shows the crystal structures of $PbPdO_2$. For systems involving magnetic calculations, spin polarization calculation was adopted. All the atoms were fully relaxed lower than 0.02 eV/Å.

3. Results and discussion

Fig. 2 shows the XRD patterns of $PbPdO_2$ and $PbPd_{0.9}M_{0.1}O_2$ (M = Cu, Co, Fe) films. All the samples were well confirmed with the standard PDF (No. 38-1357). They are single phase with the body-centered orthorhombic structure. The diffraction peaks were observed at 2θ = 26.27°, 31.55° and 38.65° correspond to (1 1 1)*, (2 1 1), and (0 0 2) planes of $PbPdO_2$ phase, respectively. And the peak that at 2θ = 38.65° has the strongest intensity. Apparently, all the samples have (0 0 2) preferred direction which is similar with the results in Ref. [5]. Especially, compared to the standard PDF (25.17°), the peak around 2θ = 26.27° has 1.1° shift to larger angle and it can be explained as the follows: The lattice constant of (1 0 0) oriented MgO single crystal is 4.212 Å, which is close to (0 0 2) oriented $PbPdO_2$ (c = 4.66 Å). When the thickness of film is small, the samples are more likely to grow along the (1 0 0) plane. As a result, the lattice mismatch may exist in the samples. According to our calculations, the lattice mismatch will make the (1 1 1) peak shift to higher angle [13]. Thus, the peak around 2θ = 26.27° can be attributed to the (1 1 1) planes of $PbPdO_2$ phase.

Fig. 3 is the Raman spectra of $PbPdO_2$ and $PbPd_{0.9}M_{0.1}O_2$ (M = Cu, Co, Fe) films. From the figure, only two main peaks (around 127 cm^{-1} and 567 cm^{-1}) were observed in $PbPdO_2$ film which correspond to the vibration modes in the structure of $PbPdO_2$ [12]. For the three doped samples, one more peak was detected besides the above-mentioned ones. The peak around 650 cm^{-1} can be assigned to the B1g mode of Pd-O in single crystal PdO. Apparently, Cu, Co and Fe dopants do have the evident influence on Pd-O bonding state. For $Pb(Pd,Fe)O_2$ sample, there was another peak around 471 cm^{-1} was detected, which needs further to be investigated. So far, the study in the microstructure of $PbPdO_2$ is seldom, so the explanation of the Raman results needs to be further depicted in theoretically.

Fig. 4 displays the SEM images of $PbPdO_2$ and $PbPd_{0.9}M_{0.1}O_2$ (M = Cu, Co, Fe) films. From the figure, one notices that, the $PbPdO_2$ film exhibits a nanograin structure, and the average grain size reached about 20 nm, which is similar to the results from Su et al. [4]. Moreover, it is obviously observed that the surface morphologies of the samples are changed from granular structure to rod-like structure after Cu, Co and Fe dopants. The length of rod reaches about 200 nm and the density of the films is decreased.

Table 1 lists the element concentrations of $PbPdO_2$ and $PbPd_{0.9}M_{0.1}O_2$ (M = Cu, Co, Fe) films from EDS measured results. The Pb:(Pd + M) atomic ratios are 0.81, 0.71, 0.79, 0.85 for $PbPdO_2$ and $PbPd_{0.9}Cu_{0.1}O_2$, $PbPd_{0.9}Co_{0.1}O_2$ and $PbPd_{0.9}Fe_{0.1}O_2$, respectively. Apparently, some Pb vacancies exist in all samples and they can be caused by the volatilization of Pb during the heating process. Moreover, the $PbPd_{0.9}Cu_{0.1}O_2$ possessed most Pb vacancies, and Pb vacancies in $PbPd_{0.9}Fe_{0.1}O_2$ are fewest.

To determine the valence state of the elements in the samples, the X-ray photoelectron spectra (XPS) were measured. Fig. 5 illustrates the XPS spectra at Pd 3d for $PbPdO_2$ and $PbPd_{0.9}M_{0.1}O_2$ (M = Cu, Co, Fe)

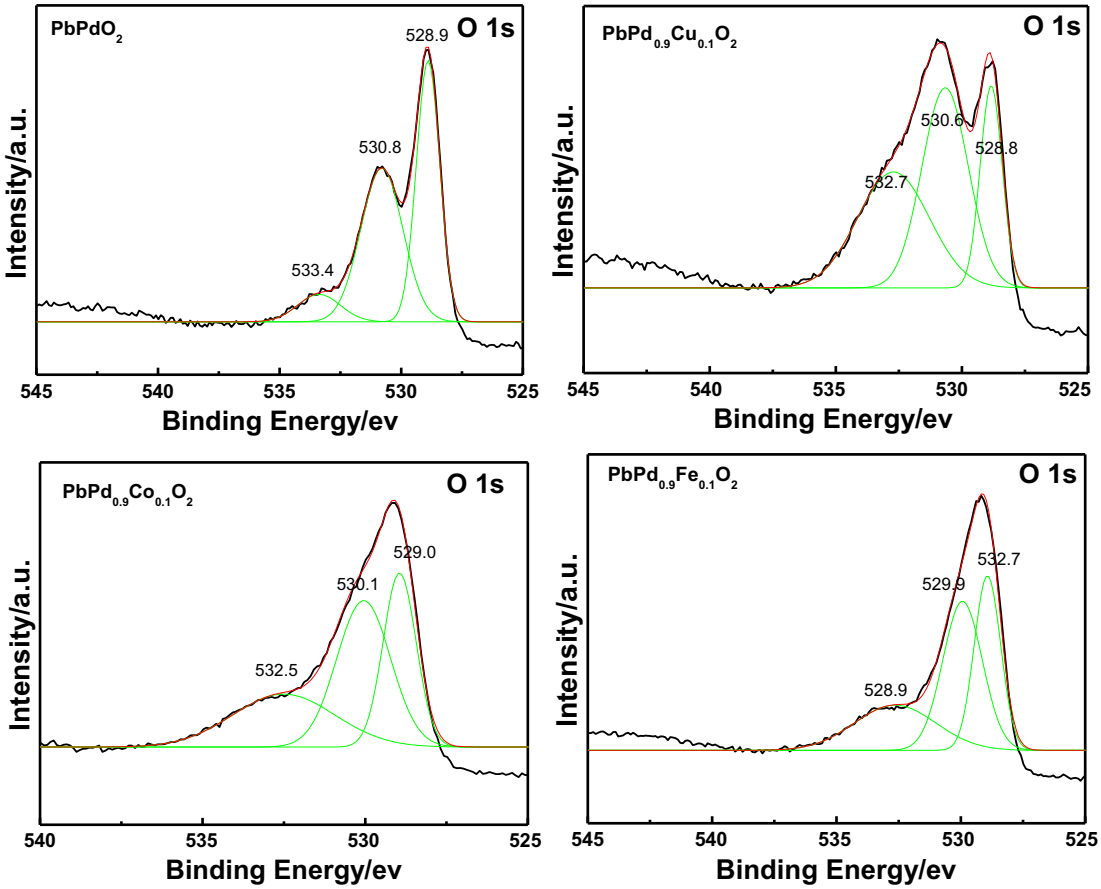

Fig. 7. XPS spectra of O 1s for $PbPdO_2$ and $PbPd_{0.9}M_{0.1}O_2$ (M = Cu, Co, Fe) films.

films. The energy scale was calibrated by assigning 284.8 eV to the C1s peak. From the figure, one can see that the peaks for Pd 3d are symmetric and centered at around 336 eV and 342 eV, standing for Pd $3d_{5/2}$ and Pd $3d_{3/2}$ respectively. The two peaks can be attributed to the formation of Pd^{2+} [14,22,35,36].

The XPS spectra of Pb 4f for $PbPdO_2$ and $PbPd_{0.9}M_{0.1}O_2$ (M = Cu, Co, Fe) films are shown in Fig. 6. The binding energy of Pb 4f contains 2 peaks, coming from the excitation of Pb $4f_{5/2}$ and Pb $4f_{7/2}$, respectively [12,22]. The Pb $4f_{5/2}$ spectra (the high BE line) can be separated into two characteristic peaks: a main peak at 141.3 eV and a satellite peak at 142.5 eV. Similarly, the Pb $4f_{7/2}$ (the lower BE line) spectra can be decomposed into two peaks: a main peak at 136.4 eV and a satellite peak at 137.5 eV. Both main peaks can be attributed to the lattice Pb (Pb^{2+}), while both satellite peaks can be assigned to Pb vacancy. According to the results of peak area percentage, $PbPd_{0.9}Cu_{0.1}O_2$ contains most Pb vacancies, while $PbPd_{0.9}Fe_{0.1}O_2$ sample has fewest ones. These results on the Pb vacancy are consistent with EDS measured data in Table 1.

The XPS spectra of O 1s for $PbPdO_2$ and $PbPd_{0.9}M_{0.1}O_2$ (M = Cu, Co, Fe) films are shown in Fig. 7. The shape of O 1s spectra can be decomposed into three peaks: a main peak at around 529 eV (named as peak I) and two satellite peaks at around 530.5 (529.9 ~ 530.8) eV (named as peak II) and 532.8 (532.5 ~ 533.4) eV (named as peak III). The peak I can be assigned to the lattice O in $PbPdO_2$. The satellite peaks II and III can be assigned to surface absorbed oxygen and hydroxyl, respectively [12,27,28]. Especially, the peak III can be associated with Pb vacancy, which can be explained as following: the valence state of Pb shifts from +2 to +0 due to Pb vacancy, which makes the superfluous O^{2-} to be oxidized to O^{1-}. As a result, the O^{1-} will absorb hydroxyl and CO_2. Therefore, the surfaces of the samples will absorb hydroxyl and CO_2 after explosion to the atmosphere. From the measured XPS spectra, it is obtained that the area percentages of the peak III for $PbPdO_2$ and $PbPd_{0.9}M_{0.1}O_2$ (M = Cu, Co, Fe) films are 8%, 37%, 28% and 25%, respectively. Thus, the content of Pb vacancies in undoped $PbPdO_2$ is lowest. Doping increases the content of Pb vacancies, and Cu doping makes the sample to attain most Pb vacancies. These results are also consistent with the EDS results above.

The XPS spectra of 2*p* states of Cu, Co and Fe for $PbPd_{0.9}M_{0.1}O_2$ films are shown in Fig. 8. For $PbPd_{0.9}Cu_{0.1}O_2$, the peaks locate at 952.08 eV and 932.26 eV correspond to $2p_{1/2}$ and $2p_{3/2}$ of Cu^{1+}, respectively [37]. Thus, the valence state of Cu ion in the sample should be +1. For $PbPd_{0.9}Co_{0.1}O_2$, the binding energy of 796.1 eV and 781.0 eV correspond respectively to $2p_{1/2}$ and $2p_{3/2}$ of Co^{2+}, while the 794.7 eV and 779.6 eV correspond to $2p_{1/2}$ and $2p_{3/2}$of Co^{3+} [38–40]. These results are similar with that in Co_3O_4 [41,42]. It is reasonable to deduce that the valence state of Co ion in our sample is also a mixed one. For $PbPd_{0.9}Fe_{0.1}O_2$, the peaks locate at 710.7 eV and 724 eV can be assigned to $2p_{3/2}$ and $2p_{1/2}$ of Fe^{3+} [43]. The valence state of Fe ion in the sample is considered to be +3.

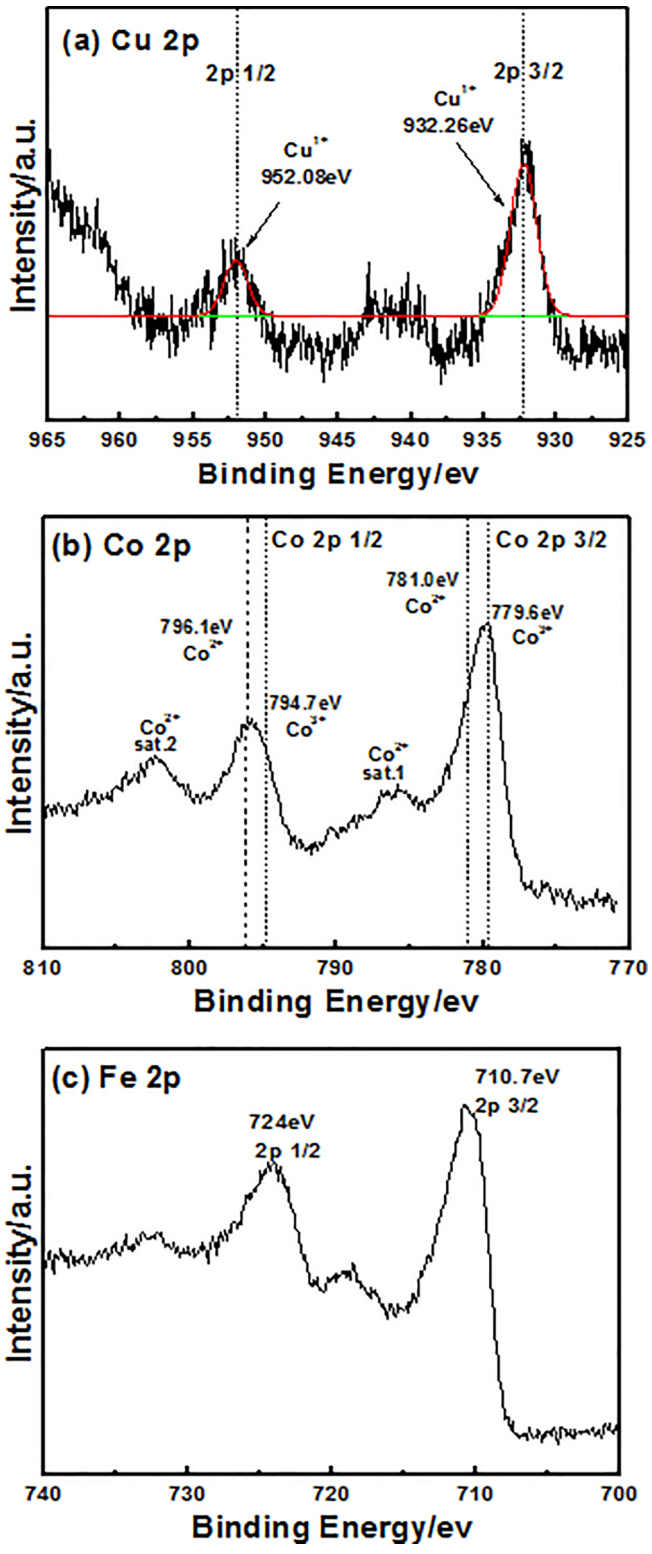

Fig. 8. XPS spectra of Cu 2p (a), Co 2p (b) and Fe 2p (c) for $PbPd_{0.9}M_{0.1}O_2$ (M = Cu, Co, Fe) films.

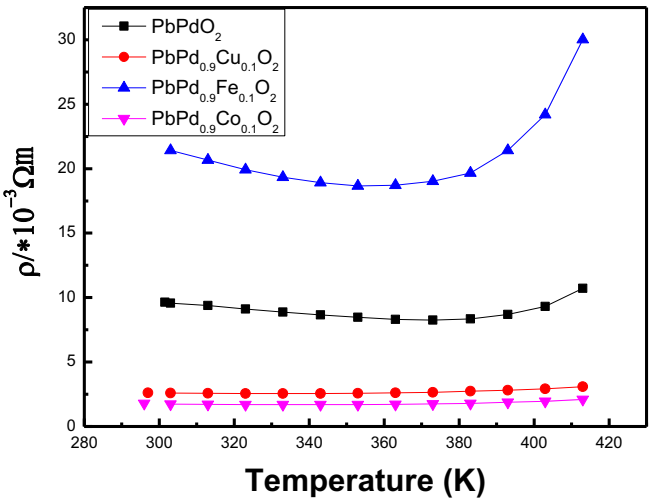

Fig. 9. Temperature dependence of resistivity for $PbPdO_2$ and $PbPd_{0.9}M_{0.1}O_2$ (M = Cu, Co, Fe) films.

Fig. 9 shows the temperature dependence of the electrical resistivity (ρ) for $PbPdO_2$ and $PbPd_{0.9}M_{0.1}O_2$ (M = Cu, Co, Fe) films. The individual enlarged figures are shown in Fig. 10. From the figures, it is found that, the Cu and Co dopants have ρ value of $PbPdO_2$ reduce, while the Fe dopant has ρ value of $PbPdO_2$ enhance. Therefore, doping has an evident influence on the electric properties of $PbPdO_2$. In addition, it can be noticed that all samples possess a wide temperature of metal-insulator transition (T_{MI}) at around 330–370 K. The values of T_{MI} for $PbPdO_2$ and $PbPd_{0.9}M_{0.1}O_2$ (M = Cu, Co, Fe) films are respectively 370 K, 333 K, 342 K and 353 K, which means that doping makes the value of T_{MI} to be reduced. The high value of T_{MI} are similar to the experimental that in Ref. [9], but much higher than other reports [3–7,14]. This clear difference of T_{MI} may be associated with the various microstructures resulting from the different prepared conditions. The underlying mechanism calls for further study.

Fig. 11 shows the *M-H* hysteresis loops (at room temperature) for $PbPdO_2$ and $PbPd_{0.9}M_{0.1}O_2$ (*M* = Cu, Co, Fe) films. All samples exhibit room ferromagnetism. The saturation magnetization values for $PbPdO_2$ and $PbPd_{0.9}M_{0.1}O_2$ (M = Cu, Co, Fe) films are 1.95 emu/cm^{-3}, 2.4 emu/cm^{-3}, 3.2 emu/cm^{-3} and 15.8 emu/cm^{-3}, respectively. Apparently, doping enhances the magnetism of $PbPdO_2$ film, and Fe doping increases evidently the magnetization of $PbPdO_2$.

In theory, the valence state of Pd in $PbPdO_2$ is supposed to be +2, so the highest filled orbital of Pd^{2+} is d_{xy} [5] and it is filled with a pair of spin-up and -down electrons. Thus, the expected effective spin magnetic moment is zero. The weak magnetism in our samples can be explained as follows. From the EDS and XPS results above, one can see that Pb vacancies exist in the samples, and they are supposed to be the origin of the magnetism. Due to the existence of Pb vacancies, the valence state of Pb shift from +2 to +0, making O^{2-} oxide to O^{1-}. The outer electron of O^{1-} is $2p^5$, contributing 1 μ_B to magnetic moment. Fig. 12 demonstrates density of states (DOS) of pure $PbPdO_2$ with Pb vacancy (Pb^{2-}) and $Pb(Pd,M)O_2$ (M = Cu^{1+}, $Co^{2+,3+}$, and Fe^{3+}) films from first-principles calculations. The calculated results indicate that Pb vacancy (Pb^{2-}) may induce magnetism in $PbPdO_2$, with 2.81 μ_B for the system. For doped samples, the magnetism should

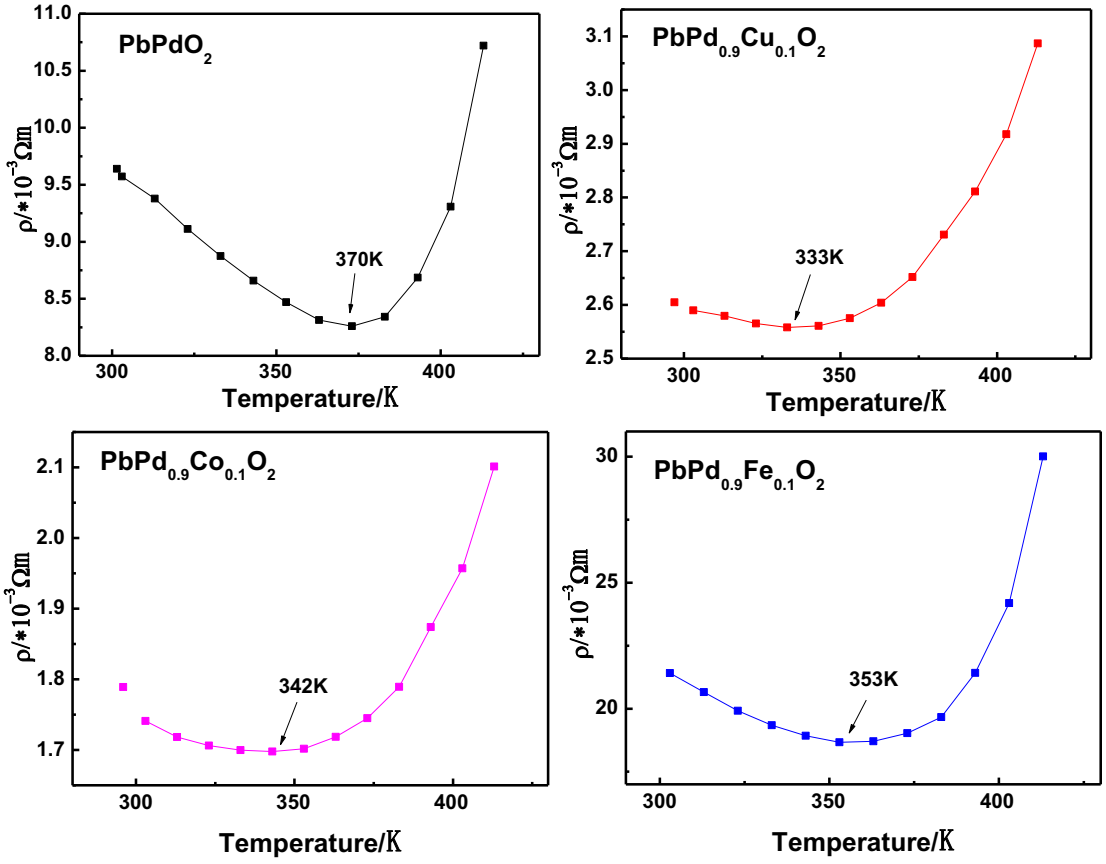

Fig. 10. Temperature-dependent resistivity of $PbPdO_2$ and $PbPd_{0.9}M_{0.1}O_2$ (M = Cu, Co, Fe) films.

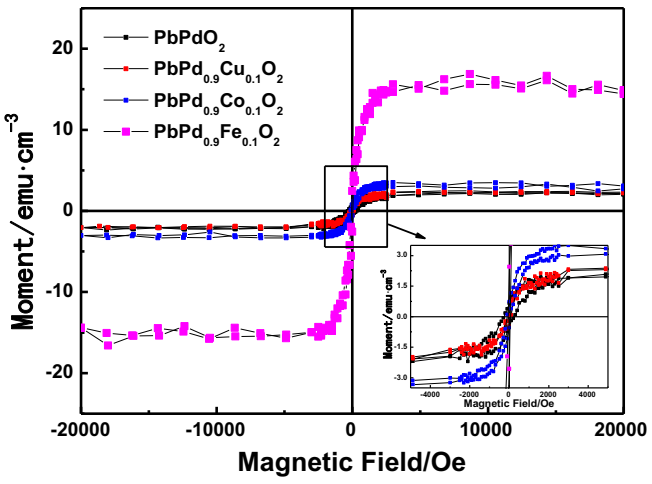

Fig. 11. *M-H* curves at room temperature (300 K) for $PbPdO_2$ and $PbPd_{0.9}M_{0.1}O_2$ (M = Cu, Co, Fe) films.

come from two ways: Pb vacancies and effective moment from the doped ion. Fe^{3+} doped $PbPdO_2$ is found to have a largest magnetic moment up to 10.92 μ_B, while $Co^{2+,3+}$ and Cu^{1+} dopants produce magnetic moments of 9.46 μ_B and 6.03 μ_B, respectively. The calculated results are consistent with the measured ones in Fig. 11.

Moreover, from Fig. 12(a), $PbPdO_2$ with Pb vacancy (Pb^{2-}) is insulating with the band gap of 0.028 eV. As Cu^{1+} and $Co^{2+,3+}$ doped, the band gap of $PbPdO_2$ reduced to 0.01 and 0.008 eV in Fig. 12(b) and (c), respectively. This result indicates an increase in the conductivity of the Cu and Co doped system, which is also verified by the resistance measurement in Fig. 9. Fe^{3+} doped film, on the contrary, increase the band gap of $PbPdO_2$ to 0.032 eV from Fig. 12(d), which is also consistent with experimental result in Fig. 9. In addition, for $PbPd_{0.9}Co_{0.1}O_2$, the valence state of Co is a mix of +2 and +3. No Co cluster exists in the sample, so the magnetism is not caused by Co cluster. On the other hand, the oxide of Co is nonmagnetic. Thus, the magnetism detected in the $PbPd_{0.9}Co_{0.1}O_2$ sample are intrinsic. It results from the Co getting into the lattice of $PbPdO_2$.

To understand the magnetism of $PbPdO_2$ in depth, ZFC-FC M-T curves were measured at a magnetic field of 100Oe and they are shown in Fig. 13. Apparently, as the temperature decreases from 360 K to 70 K, the FC and ZFC curves diverges from each other, indicating that the coexistence of the ferromagnetism, paramagnetism and antiferromagnetism in the samples [22]. When it rises to around 350 K, two curves merge gradually, indicating that the ferromagnetism in the samples persists up to around 360 K. The results are consistent with the other those [11,22].

4. Conclusions

We prepared $PbPdO_2$ and $PbPd_{0.9}M_{0.1}O_2$ (M = Cu, Co, Fe) films

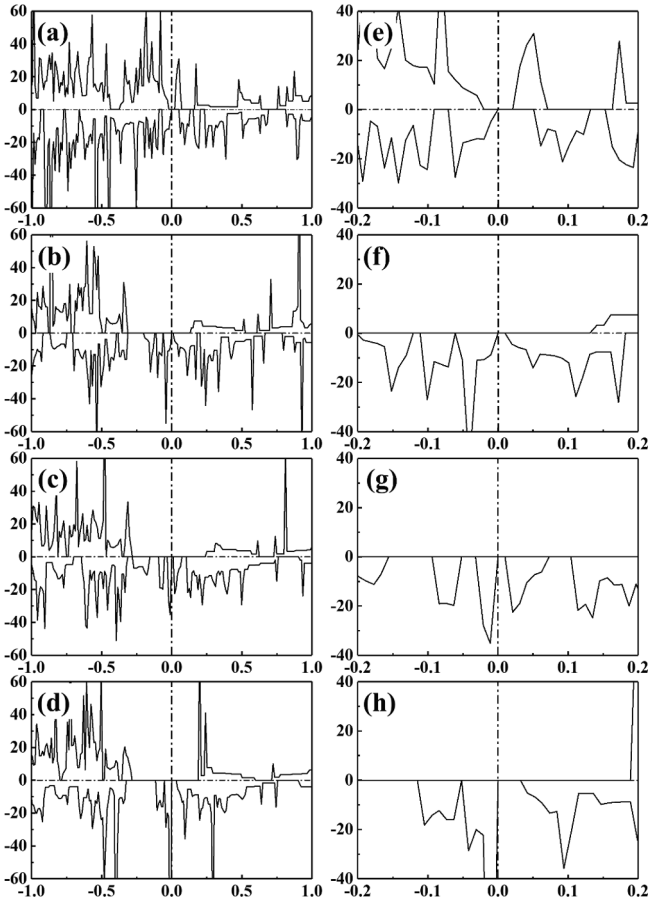

Fig. 12. Density of states of (a) (b) pure $PbPdO_2$ with Pb vacancy (V_{Pb}^{2-}) and (c) (d) Cu^{+}, (e) (f) $Co^{2+,3+}$, (g) (h) Fe^{3+} doped $PbPdO_2$ films with Pb vacancy. (b), (d), (f) and (h) are the magnified views of the corresponding DOS. The dotted line represents the Fermi level.

using PLD technique. XRD, Raman, SEM, XPS, AFM and VSM measured results indicate that $PbPdO_2$ film can be well fabricated, magnetic atoms Cu, Co and Fe can be introduced into (0 0 2) orientation preferred $PbPdO_2$ film. We found the valence states of M in $PbPd_{0.9}M_{0.1}O_2$ (M = Cu, Co, Fe) films were Cu^{1+}, Co^{2+} and Co^{3+} coexistence and Fe^{3+}, respectively. Ferromagnetism was measured for $PbPdO_2$ and $PbPd_{0.9}M_{0.1}O_2$ (M = Cu, Co, Fe) films with high metal-insulator transition temperatures at around 330–370 K. Moreover, $PbPd_{0.9}Fe_{0.1}O_2$ has largest electrical resistivity and magnetic moment, and $PbPd_{0.9}M_{0.1}O_2$ (M = Cu, Co) have more magnetic moment and lower resistivity than $PbPdO_2$ film. The changes of electrical and magnetic properties due to dopant has been also confirmed by our first-principles calculations.

Acknowledgements

Our work is supported by the National Natural Science Foundation of China (Nos. 61574037, 11874113, 61804030), the Natural Science Foundations of Fujian Province of China (Nos. 2017J06001, 2016J05151, J2016J01011). Science and Technology Major Projects of Fujian Province (2013HZ0003), Project of Fujian Development and Reform Commission (2013-577).

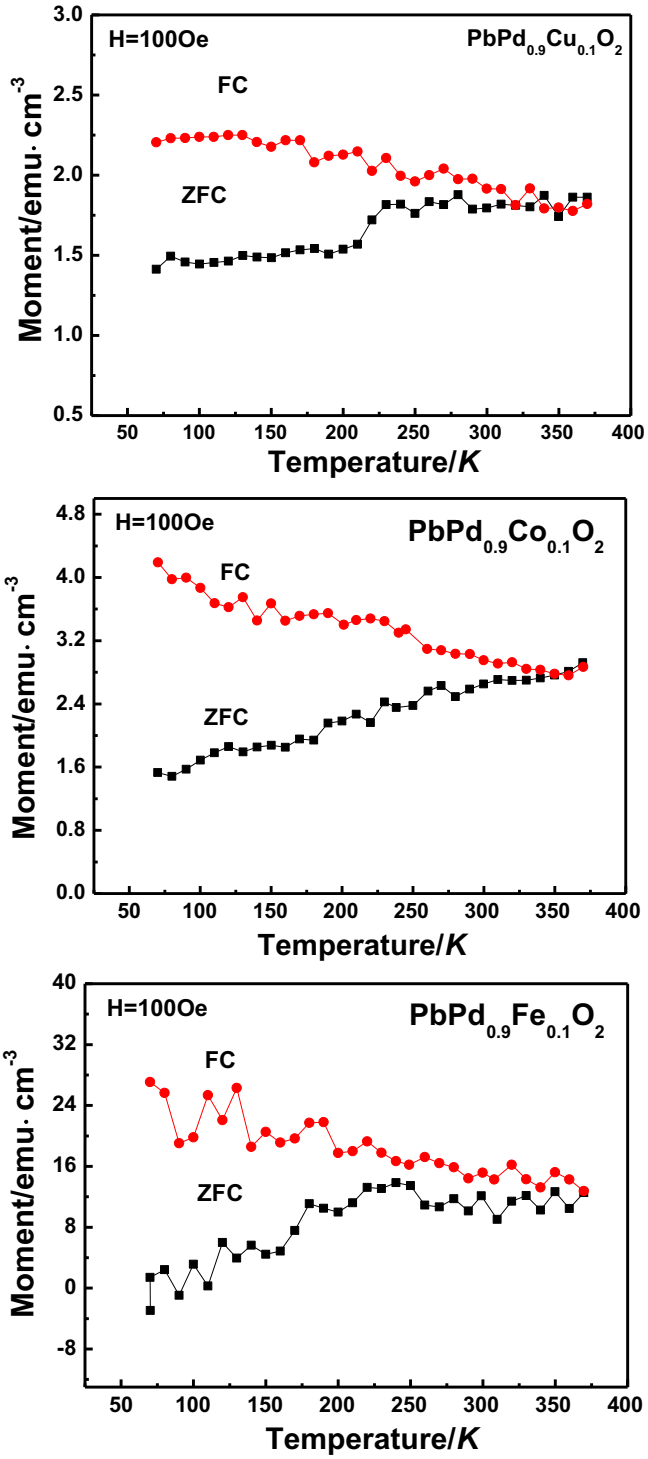

Fig. 13. ZFC-FC *M-T* curves for $PbPdO_2$ and $PbPd_{0.9}M_{0.1}O_2$ (M = Cu, Co, Fe) films.

References

[1] X.L. Wang, Proposal for a new class of materials: spin gapless semiconductors, Phys. Rev. Lett. 100 (2008) 3136–3140.
[2] X.L. Wang, Dirac spin-gapless semiconductors: promising platforms for massless and dissipationless spintronics and new (quantum) anomalous spin Hall effects, Natl. Sci. Rev. 4 (2017) 252–257.
[3] X.L. Wang, S.X. Dou, C. Zhang, Zero-gap materials for future spintronics, electronics and optics, NPG Asia Mater. 2 (2010) 31–38.

[4] H.L. Su, S.Y. Huang, Y.F. Chiang, J.C.A. Huang, C.C. Kuo, Y.W. Du, Y.C. Wu, R.Z. Zuo, Unusual high-temperature ferromagnetism of $PbPd_{0.81}Co_{0.19}O_2$ nanograin film, Appl. Phys. Lett. 99 (2011) (102508–102508–3).
[5] X.L. Wang, G. Peleckis, C. Zhang, H. Kimura, S. Dou, Colossal electroresistance and giant magnetoresistance in doped $PbPdO_2$ thin films, Adv. Mater. 21 (2009) 2196–2199.
[6] S.W. Chen, S.C. Huang, G.Y. Guo, S. Chiang, J.M. Lee, S.A. Chen, S.C. Haw, K.T. Lu, J.M. Chen, A combined first principle calculations and experimental study on the spin-polarized band structure of Co-doped $PbPdO_2$, Appl. Phys. Lett. 101 (2012) (222104–222104–4).
[7] P. Srivastava, B.J. Nagare, D.G. Kanhere, P. Sen, Electronic structure of the spin gapless material Co-doped $PbPdO_2$, J. Appl. Phys. 114 (2013) (103709–103709–8).
[8] D.H. Kim, J. Hwang, E. Lee, K.J. Lee, S.M. Choo, M.H. Jung, J. Baik, H.J. Shin, B. Kim, K. Kim, B.I. Min, J.S. Kang, Valence states and electronic structures of Co and Mn substituted spin gapless semiconductor $PbPdO_2$, Appl. Phys. Lett. 104 (2014) (022411–022411–4).
[9] S.M. Choo, K.J. Lee, S.M. Park, J.B. Yoon, G.S. Park, C.Y. You, M.H. Jung, Crossover between weak anti-localization and weak localization by Co doping and annealing in gapless $PbPdO_2$ and spin gapless Co-doped $PbPdO_2$, Appl. Phys. Lett. 106 (2015) (172404–172404–3).
[10] K. Lee, S.M. Choo, M.H. Jung, Magnetic versus nonmagnetic ion substitution effects in gapless semiconductor $PbPdO_2$, Appl. Phys. Lett. 106 (2015) (072406–072406–3).
[11] T.T. Song, F.L. Tang, H.L. Su, P.Y. Chuang, J. Liu, C. Mei, S.Y. Huang, M.K. Lee, J.C.A. Huang, Y.C. Wu, Microstructure and magnetism of sol-gel synthesized Co doped $PbPdO_2$ nanograin film, J. Magn. Magn. Mater. 407 (2016) 37–41.
[12] X. Chen, Y. Chen, Y. Yang, H. Jia, J.M. Zhang, S. Chen, Z. Huang, The structure and electrical properties of $PbPdO_2$ thin films with preferred orientation prepared by PLD, Ceram. Int. 43 (2017) 10428–10433.
[13] Y. Yang, K. Zhong, G. Xu, J.M. Zhang, Z. Huang, Electronic structure and its external electric field modulation of $PbPdO_2$ ultrathin slabs with (002) and (211) preferred orientations, Sci. Rep. 7 (2017) (6898–6898–7).
[14] J.A. Kurzman, M.S. Miao, R. Seshadri, Hybrid functional electronic structure of $PbPdO_2$, a small-gap semiconductor, J. Phys.: Condens. Matter 23 (2011) (465501–465501–7).
[15] X. Wang, Z. Cheng, J. Wang, X.L. Wang, G. Liu, Recent advances in the Heusler based spin-gapless semiconductors, J. Mater. Chem. C 4 (2016) 7176–7192.
[16] L. Bainsla, A.I. Mallick, M. Manivel Raja, A.K. Nigam, B.S.D.Ch.S. Varaprasad, Y.K. Takahashi, A. Alam, K.G. Suresh, K. Hono, Spin gapless semiconducting behavior in equiatomic quaternary CoFeMnSi Heusler alloy, Phys. Rev. B 91 (2015) (104408–104408–4).
[17] S. Ouardi, G.H. Fecher, C. Felser, J. Kubler, Realization of spin gapless semiconductors: the Heusler compound Mn_2CoAl, Phys. Rev. Lett. 110 (2013) (100401–100401–5).
[18] L. Bainsla, A.I. Mallick, M. Manivel Raja, A.A. Coelho, A.K. Nigam, D.D. Johnson, Aftab Alam, K.G. Suresh, Origin of spin gapless semiconductor behavior in CoFeCrGa: theory and experiment, Phys. Rev. B 92 (2015) (045201–045201–5).
[19] Y. Du, G.Z. Xu, X.M. Zhang, Z.Y. Liu, S.Y. Yu, E.K. Liu, W.H. Wang, G.H. Wu, Crossover of magnetoresistance in the zero-gap half-metallic Heusler alloy Fe_2CoSi, EPL (Europhys. Lett.) 103 (2013) (37011–37011–6).
[20] K.J. Lee, S.M. Choo, J.B. Yoon, K.M. Song, Y. Saiga, C.-Y. You, N. Hur, S.I. Lee, T. Takabatake, M.H. Jung, Magnetic properties of gapless semiconductors: $PbPdO_2$ and $PbPd_{0.9}Co_{0.1}O_2$, J. Appl. Phys. 107 (2010) (09C306–09C306–3).
[21] K.J. Lee, S.M. Choo, Yuta Saiga, Toshiro Takabatake, Myung-Hwa Jung, Magnetic properties of Mn and Co doped $PbPdO_2$, J. Appl. Phys. 109 (2011) (07C316–07C316–3).
[22] F.L. Tang, J. Liu, C. Mei, S.Y. Huang, T.T. Song, H.L. Su, M.K. Lee, Y.C. Wu, J.C.A. Huang, Microstructure and magnetism of Co-doped $PbPdO_2$ films with different grain sizes, RSC Adv. 6 (2016) 37522–37529.
[23] S.W. Chen, S.C. Huang, G.Y. Guo, J.M. Lee, S. Chiang, W.C. Chen, Y.C. Liang, K.T. Lu, J.M. Chen, Gapless band structure of $PbPdO_2$: a combined first principles calculation and experimental study, Appl. Phys. Lett. 99 (2011) (012103–012103–3).
[24] S.M. Choo, K.J. Lee, S.M. Park, G.S. Park, M.H. Jung, Annealing effect on surface morphology and electrical transport of $PbPdO_2$ and Pb(Pd, Co)O_2, J. Appl. Phys. 113 (2013) (014904–014904–4).
[25] T.C. Ozawa, T. Taniguchi, Y. Nagata, Y. Noro, T. Naka, A. Matsushita, Metal–insulator transition and large thermoelectric power of a layered palladium oxide: $PbPdO_2$, J. Alloys Compd. 388 (2005) 1–5.
[26] T.C. Ozawa, T. Taniguchi, Y. Nagata, Y. Noro, T. Naka, A. Matsushita, Cu doping and pressure effect on a layered palladium oxide: $PbPdO_2$, J. Alloys Compd. 395 (2005) 32–35.
[27] J. Liu, C. Mei, P.Y. Chuang, T.T. Song, F.L. Tang, H.L. Su, J.C.A. Huang, Y.C. Wu, Effect of Fe doping on the magnetic properties of $PbPdO_2$ nanograin film fabricated by sol-gel method, Ceram. Int. 42 (2016) 15762–15766.
[28] F. Tang, C. Mei, P. Chuang, T. Song, H. Su, Y. Wu, Y. Qiao, J.C.A. Huang, Y.F. Liao, Valence state and magnetism of Mn-doped $PbPdO_2$ nanograin film synthesized by sol-gel spin-coating method, Thin Solid Films 623 (2017) 14–18.
[29] C. Mei, J. Liu, P.Y. Chuang, T.T. Song, F.L. Tang, H.L. Su, J.C.A. Huang, Y.C. Wu, High-temperature ferromagnetism of Ni-doped $PbPdO_2$ nanograin films synthesized by sol-gel spin-coating method, Ceram. Int. 43 (2017) 1997–2003.
[30] G. Kresse, J. Hafner, Ab initio molecular dynamics for open-shell transition metals, Phys. Rev. B 48 (1993) 13115–13118.
[31] G. Kresse, J. Furthmüller, Efficient iterative schemes for ab initio total-energy calculations using a plane-wave basis set, Phys. Rev. B 54 (1996) 11169.
[32] P.E. Blöchl, Projector augmented-wave method, Phys. Rev. B 50 (1994) 17953–17979.
[33] G. Kresse, J. Furthmüller, Efficiency of ab-initio total energy calculations for metals and semiconductors using a plane-wave basis set, Comput. Mater. Sci. 6 (1996) 15–50.
[34] J.P. Perdew, K. Burke, M. Ernzerhof, Generalized gradient approximation made simple, Phys. Rev. Lett. 77 (1996) 3865–3868.
[35] K.C. Lee, Y.J. Chiang, Y.C. Lin, F.M. Pan, Effects of PdO decoration on the sensing behavior of SnO_2 toward carbon monoxide, Sens. Actuators, B 226 (2016) 457–464.
[36] M. Brun, A. Berthet, J.C. Bertolini, XPS, AES and Auger parameter of Pd and PdO, J. Electron Spectrosc. Relat. Phenom. 104 (1999) 55–60.
[37] S. Velu, K. Suzuki, C.S. Gopinath, Photoemission and in situ XRD investigations on CuCoZnAl-mixed metal oxide catalysts for the oxidative steam reforming of methanol, J. Phys. Chem. B 106 (2002) 12737–12746.
[38] J.E. Ghoul, M. Kraini, O.M. Lemine, L.E. Mir, Sol-gel synthesis, structural, optical and magnetic properties of Co-doped ZnO nanoparticles, J. Mater. Sci.: Mater. Electron. 26 (2015) 1–8.
[39] X.F. Wang, J.B. Xu, B. Zhang, H.G. Yu, J. Wang, X.X. Zhang, J.G. Yu, Q. Li, Signature of intrinsic high-temperature ferromagnetism in cobalt-doped zinc oxide nanocrystals, Adv. Mater. 18 (2006) 2476–2480.
[40] V. Singh, D.T. Major, Electronic structure and bonding in Co-based single and mixed valence oxides: a quantum chemical perspective, Inorg. Chem. 55 (2016) 3307–3315.
[41] W.L. Roth, The magnetic structure of Co_3O_4, J. Phys. Chem. Solids 25 (1964) 1–10.
[42] Y. Ichiyanagi, Y. Kimishima, S. Yamada, Magnetic study on Co_3O_4 nanoparticles, J. Magn. Magn. Mater. 272–276 (2004) e1245–e1246.
[43] T. Yamashita, P. Hayers, Analysis of XPS spectra of Fe^{2+} and Fe^{3+} ions in oxide materials, Appl. Surf. Sci. 254 (2008) 2441–2449.